Antibody-induced crosslinking immobilizes acetylcholine receptors.

Mobile receptors exhibit anomalous, cholesterol-sensitive diffusion and clustering

Alejo Mosqueira, Pablo A. Camino and Francisco J. Barrantes*

Laboratory of Molecular Neurobiology, Biomedical Research institute (BIOMED),

UCA–CONICET, Av. Alicia Moreau de Justo 1600, C1107AFF Buenos Aires, Argentina.

*Address correspondence to: F.J. Barrantes, Laboratory of Molecular Neurobiology, BIOMED UCA-CONICET, Av. Alicia Moreau de Justo 1600, C1107AFF, Buenos Aires, Argentina.

E-mail: francisco_barrantes@uca.edu.ar

Short title: Antibody-acetylcholine receptor diffusion

The abbreviations used are: BTX, α-bungarotoxin; mAb, monoclonal antibody; nAChR, nicotinic acetylcholine receptor; CDx, methyl-β-cyclodextrin; CDx-Chol, cholesterol-methyl-β-cyclodextrin complex; MSD, mean-squared displacement; SPT, single-particle tracking.

KEYWORDS: antibody-receptor crosslinking; antigenic modulation; superresolution microscopy; cholesterol; single-molecule tracking; lateral diffusion; acetylcholine receptor dynamics; antibody-receptor interactions.

Abstract

Synaptic strength depends on the number of cell-surface neurotransmitter receptors in dynamic equilibrium with intracellular pools. Dysregulation of this homeostatic balance occurs e.g. in myasthenia gravis, an autoimmune disease characterized by a decrease in the number of postsynaptic nicotinic acetylcholine receptors. Monoclonal antibody mAb35 mimics this effect. Using STORM nanoscopy we characterize the individual and ensemble dynamics of mAb35-crosslinked receptors. Antibody labeling of live cells results in 80% receptor immobilization. The remaining mobile fraction exhibits a heterogeneous combination of Brownian and anomalous diffusion. Single-molecule trajectories exhibit a two-state switching behavior between free Brownian walks and anticorrelated walks within confinement zones. The latter act as permeable fences (~34 nm radius, ~400 ms lifetime). Dynamic clustering, trapping and immobilization also occur in larger areas (~150 nm radius) with longer lifetimes (11 ± 1 s), in a strongly cholesterol-sensitive manner. Cholesterol depletion increases the size and average duration of the clustering phenomenon; cholesterol enrichment has the opposite effect. The disclosed high proportion of mAb35-crosslinked immobile receptors, together with their anomalous, cholesterol-sensitive diffusion and clustering, provides new insights into the antibody-enhanced antigenic modulation that leads to physiopathological internalization and degradation of receptors in myasthenia.

Introduction

The nicotinic acetylcholine receptor (nAChR) is one of the most ubiquitous neurotransmitter receptor proteins in both peripheral and central nervous systems of vertebrates (for a recent review see (Changeux 2018)). This pentameric ligand-gated ion channel intervenes in a variety of physiological processes and is subject to dysfunction in pathological conditions such as chronic pain, schizophrenia spectrum disorders, Alzheimer disease, Parkinson disease, or neurological autoimmune diseases like myasthenia gravis. In the latter, about two-thirds of the autoantibodies found in myasthenic patients are directed against the so-called main immunogenic region (MIR) of the muscle-type nAChR (Tzartos et al. 1988). This finding resulted from the introduction of libraries of cloned hybridoma cell lines producing monoclonal antibodies into the individual nAChR subunits and regions thereof (Tzartos and Lindstrom 1980). mAb35, the antibody used in the present study, is an IgG1 immunoglobulin isotype reacting with the MIR epitope located on the extracellular surface of the nAChR α1 subunit (Tzartos et al. 1991). This monoclonal antibody was originally raised against the nAChR of *Electrophorus electricus*, the elasmobranch electric eel, and yet it competes with >75% of the serum autoantibodies obtained from humans suffering from myasthenia gravis (Tzartos et al. 1982). MIR epitopes recognized by rat mAbs consist of two discontiguous sequences, which are adjacent in the native conformation and confer high-affinity binding for rat monoclonal antibodies (Luo et al. 2009). A single IgG monoclonal antibody molecule can crosslink two nAChR molecules (Tzartos and Starzinski-Powitz 1986). Recent X-ray structural studies have confirmed that a single mAb35 molecule is able to bind two α1 subunits from two adjacent monomers -thereby crosslinking them- whereas it does not bind to the two α1 subunits within

a single nAChR monomer (Noridomi et al. 2017). Moreover, antibodies directed against the MIR of the receptor have been reported to form oligomeric complexes larger than the dimer (Conti-Tronconi et al. 1981; Tzartos et al. 1986). Ultracentrifugation and transmission electron microscopy (Barrantes 1982) and atomic force microscopy (Pissinis et al. 2015) techniques have made apparent the wide range of oligomeric forms that the nAChR can adopt in non-ionic detergent, ranging from monomers to dimers and higher oligomeric species. This structural repertoire possibly mimics a similar range of oligomeric states of the protein in situ, given the high-packing densities of the receptor in the native post-synaptic membrane, maximizing in-plane receptor-receptor contacts that favor oligomerization.

Here, we set out to explore the effects of mAb35-mediated crosslinking of the adult muscle-type nAChR heterologously expressed in a mammalian cell system on the translational dynamics and spatial organization of the protein imaged in live cells using STORM (stochastic optical reconstruction microscopy), single-molecule tracking and a combination of analytical and statistical techniques. We also analyze the impact of acute membrane cholesterol depletion (CDx) or enrichment (CDx-Chol) on the diffusion of the receptor. We account for the heterogeneous, cholesterol-dependent diffusion behavior of the nAChR in physical terms by a two-state switching model (Grebenkov 2019) between free Brownian walks and obstructed diffusion within confinement sojourns. Thus, the disclosed anomalous diffusion of the receptor crosslinked by a subclass of IgG1 antibodies known to produce severe loss of nAChR by complement-mediated lysis of the postsynaptic membrane (Vincent 2002; Paz and Barrantes 2019), appears as one of the earliest links in the chain of physiopathological events responsible for antigenic modulation, the cascade leading to enhanced nAChR internalization and

degradation, and complement-mediated lysis of the postsynaptic membrane observed in myasthenia.

Results

Antibody tagging results in a high degree of nAChR immobilization

Live CHO-K1/A5 cells labeled with the monoclonal antibody mAb35 against the nAChR α-subunit followed by Texas Red-labeled secondary antibodies were imaged under control or cholesterol-modifying conditions at a frame rate of 100 fps. Between 8 and 15 cells were recorded per condition. Reconstruction of the superresolution images and single-molecule tracking were done using the ThunderSTORM software (Ovesný et al. 2014) and the Localizer package (Dedecker et al. 2012)). Trajectories shorter than 50 temporal steps (i.e. with a difference of 50 frames between the initial and the final recorded positions) were discarded. Immobile particles were removed following the criteria of Golan and Sherman (Golan and Sherman 2017), based on the ratio of the radius of gyration and the mean step size, which is independent of the localization error. A conservative threshold ratio of 2.04 (upper 95% confidence interval) was chosen, from which a value of 80 ± 9 % was obtained for the immobile fraction of nAChRs under control conditions, as already apparent by visual inspection of the individual tracks, with no significant changes upon cholesterol modification (Suppl. Fig. 2).

Antibody-crosslinked nAChRs display ergodic-like heterogeneous diffusion

Mean squared displacement (MSD) is the most widely used criterion to detect deviations from random (Brownian) motion in protein diffusion analysis. Typically, it is studied by a

temporal-average over time (TA MSD) for single-particle trajectories or by an *ensemble*-average over several particles for the population of trajectories at a specific time (EA MSD). The nonlinear fit of the individual TA MSD yields both the anomalous exponent (β, a measure of the deviation from Brownian motion) and the generalized diffusion coefficient (K_β) (see relevant equations in Supplementary Material). A β value different from 1 is associated with anomalous (non-Brownian) diffusion: β<1 for sub-diffusion (attributed to protein-protein immobilizing interactions, confinement, or spatial inhomogeneities) and β>1 for super-diffusion (usually resulting from active cellular transport processes). At the single-molecule level, nAChR dynamics was heterogeneous: from subdiffusive to Brownian and seldom superdiffusive. The averaged β values of the population were below unity, i.e. subdiffusive, and averaged generalized diffusion coefficients K_β were in the order of 0.5 $\mu m^2 s^{-\beta}$ (Figure 1a). No significant changes were observed upon modification of cholesterol membrane content (Suppl. Fig. 3).

Single-particle analyses often require calculating temporal averages over individual trajectories from which the diffusional properties of the ensemble are calculated. Yet this is correct only under the assumption that the individual molecules can explore all accessible diffusion states within the recording time, fulfilling the ergodic hypothesis. If this assumption does not hold, the diffusional properties obtained by temporal averaging over a single molecule will not be equivalent to those resulting from ensemble averaging over the entire population. Many biological systems conform to this latter behavior and display weak ergodicity breaking (WEB), often related to transient immobilization or spatial inhomogeneities (Weigel et al. 2011; Manzo et al. 2015; Weron et al. 2017). For this reason, testing the ergodic hypothesis can unravel important features of the diffusion process. Classically, the ergodic hypothesis is

assessed by comparing the TA MSD and the EA MSD. In theory, if the system is ergodic, the TA MSD converges to the EA MSD and the parameters estimated from both averages (e.g. anomalous exponent) will be equal. However, the empirical and the theoretical values will always differ (especially for small samples), making it necessary to consider a measure of the accuracy of the empirical estimation (e.g. including the confidence interval) without which a process could be falsely classified as non-ergodic due to sample size limitations. Following this idea, we compared the EA TA MSD (ensemble average of the TA MSD) and the EA MSD together with the 95% confidence interval, as implemented in ref. (Janczura and Weron 2015). In our system, the curves of the EA TA MSD and the EA MSD appear to reflect an ergodic-like behavior (Figure 1b and Suppl. Fig. 4).

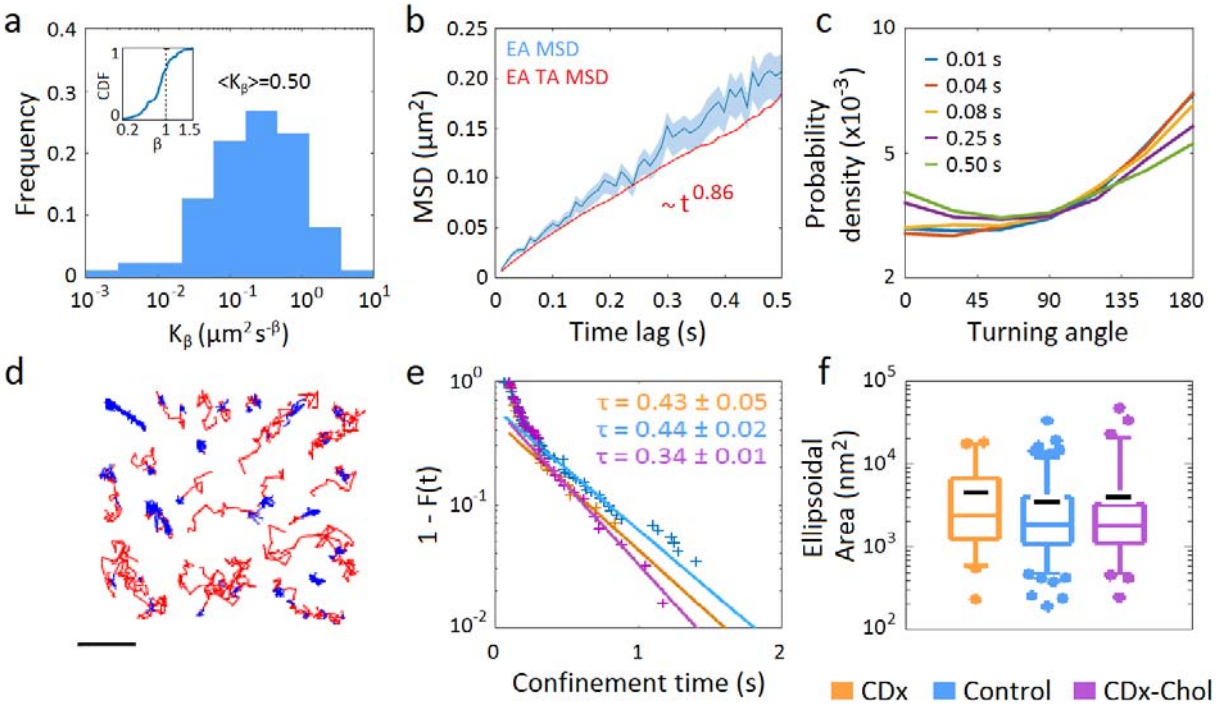

Figure 1. Mean-square displacement, turning angles and recurrence analysis applied to single-molecule nAChRs under control and cholesterol-modifying conditions. a) Frequency of the generalized diffusion coefficients (K_β) in log scale and cumulative density function of the anomalous exponent β (inset), obtained by linear regression of the temporal-averaged MSD (TA MSD) in log-log scale of single-molecule trajectories (see Methods for details). No changes were observed after modifying the membrane cholesterol content (Suppl. Fig. 3). b) The ensemble-averaged MSD (EA MSD) with the 95% confidence interval is shown in blue. An additional ensemble averaging to the TA MSD (EA TA MSD, red trace) was performed to test the ergodic hypothesis. Similar trends were observed for cholesterol-modifying conditions (see Suppl. Fig. 4). c) Probability densities of the turning angles for the (color-coded) time lags (t_{lag}) of increasing durations (10 to 500 ms). The probability density is normalized such that the integral of the curve is equal to unity. For cholesterol-modifying conditions see Suppl. Fig. 5. d) Examples of the results obtained by applying the recurrence analysis (Sikora et al. 2017) to the single-molecule nAChR trajectories. The confinement sojourns are shown in blue. Scale bar: 1 µm. e) Complementary cumulative distribution function of the resident times in the confined state for the nAChRs under control and cholesterol-modifying conditions. The distributions were exponentially tailed, with the characteristic decay times (τ) stated in the figure (in seconds). f) Ellipsoidal area of the trajectories´ portion in the confined state, obtained by fitting the confinement domain in the trajectory with an elliptic surface. Whiskers in box plots correspond to 95% confidence intervals; the limits indicate 75% confidence intervals; the black minus symbols indicate the mean and the colored horizontal lines the median in each case. The dots outside the confidence intervals are outliers.

nAChRs exhibit anticorrelated steps that conform to diffusion in a permeable fence medium

We next attempted to elucidate the biophysical process behind the ergodic-like anomalous diffusion of the nAChR. A simple way to do this is by inspecting the distribution of the directional changes or turning angles, a parameter that enabled us to analyze correlations in single-particle displacements (Burov et al. 2013). If the particles do not show any preferred direction of motion (i.e. in Brownian motion), the turning angle distribution is expected to be flat; instead, the distribution peaks at 0° if they exhibit a preference to move forward or at 180° when the preferred motion is backwards. In the present experiments, the turning angle distributions increased from 60° to reach their maximum at 180° (Figure 1c), a clear manifestation of subdiffusive random walks with anticorrelated steps (i.e. with a predilection to

retrace their steps). By numerical simulations, Krapf and coworkers analyzed the turning angle distributions of two widely tested ergodic biophysical models (Sadegh et al. 2017) that led to subdiffusion with anticorrelated steps: motion of particles in a viscoelastic fluid (fractional Brownian motion) and motion hindered by nearly immobile obstacles (obstructed diffusion). Although the turning angle distribution peaked at 180° in both models, in the first one it reached a plateau, in clear contrast with the present experimental data, indicating that nAChR dynamics is better explained by the obstructed diffusion model. Moreover, two additional properties can be obtained from inspection of the turning angle distributions. Firstly, by comparing the abruptness of the present distributions with those obtained for simulations of particles undergoing obstructed diffusion with increasing obstacle concentrations (Sadegh et al. 2017) we can infer that nAChR diffusion is hindered by a relatively high concentration of immobile particles. Secondly, we observe a significant dependence of turning angles with time lag (statistical differences between $\mathrm{t_{lag}} = 0.01$ s and $\mathrm{t_{lag}} = 0.50$ s were $p < 0.01$, for cholesterol depletion, $p < 10^{-15}$, for control and $p < 10^{-5}$, for cholesterol-enrichment conditions, respectively (see Suppl. Fig. 5). This feature was previously observed in numerical simulations of random walks in a permeable fence model (Sadegh et al. 2017), i.e. random walks within compartments of characteristic length scale and low probability of permeation. In summary, our turning angle data conform to the general depiction of molecules diffusing in a permeable fence continuum constituted by immobile obstacles at a high concentration.

Transient confinement nanodomains are a characteristic feature of nAChR motion

If receptors diffuse in a permeable fence medium with a high obstacle density (low probability of permeation), one would expect to observe motional hindrance in this medium. When a particle is confined, it tends to visit the same coordinates repeatedly until it escapes from the confinement area. Several mechanisms have been proposed to account for these trapping events (e.g. molecular crowding, protein-protein interactions, interactions with the actin cytoskeleton and membrane heterogeneities). A recently proposed analysis (Sikora et al. 2017) allows one to identify regions of confinement in individual trajectories, and extracts the characteristic sojourn durations in the recurrently-visited regions where the particle remains trapped. When applied to the nAChR trajectories, we observe that essentially all trajectories (from subdiffusive to Brownian) alternate between free walks and confinement sojourns (see Figure 1d). The residence time distribution in the confined state was exponentially tailed, with characteristic decay times of 430 ± 50 ms, 440 ± 20 ms and 340 ± 10 ms, for cholesterol depletion, control, and cholesterol enrichment conditions, respectively (Figure 1e). The average surface distended by a confinement sojourn had a radius of ~34 nm (Figure 1f), a value which was not significantly affected by changes in membrane cholesterol levels.

When we repeated the turning angle analysis on the confined and free portions of the single-molecule trajectories separately, we realized that the anticorrelated steps occurred only

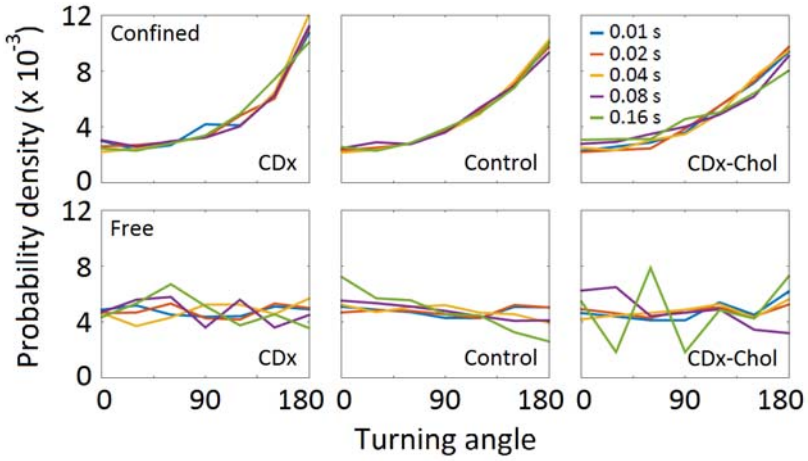

within the confined areas, whereas the free walk periods displayed a nearly flat Brownian distribution (Figure 2). An individual receptor molecule would thus appear to move freely across the cell membrane until it encounters a region of high obstacle density that hinders its movement for a certain period.

Figure 2. Turning angle probability densities of the transiently confined (upper row) and unconfined (free; bottom row) portions of the individual trajectories under control and cholesterol-modifying conditions. Probability densities for the color-coded t_{lag} of increasing durations (10 to 160 ms). The probability density is normalized such that the integral of the curve is equal to unity.

Clustering event dynamics and extension are modulated by membrane cholesterol levels

To address the possible physical nature of the immobile obstacles that hinder receptor mobility in the confinement sojourns, we examined the dynamics of cluster formation/disassembly. Using the qSR software developed by Cisse and coworkers (Cisse et al. 2013; Andrews et al. 2018), we were able to follow the temporal evolution of clustering events in live CHO-K1/A5 cells. nAChR trajectories display clustering events with an average duration of

11 ± 1 s (Figure 3a), typically followed by cluster disassembly periods. The intra-burst mean dark time (i.e. the time between two particle localizations within a clustering event) was significantly affected by cholesterol depletion, increasing from an average of 241 ± 6 ms to 274 ± 10 ms (Figure 3b). The radius of the zones where the clustering events occur was inversely proportional to cholesterol concentration, the control radius of 139 ± 6 nm increasing to 182 ± 7 nm upon cholesterol depletion and decreasing to 118 ± 7 nm with cholesterol enrichment (Figure 3c). The number of single-molecule occurrences per assembly was 50 ± 6 molecules, decreasing in a statistically significant manner to 46 ± 9 after cholesterol depletion (Figure 3d).

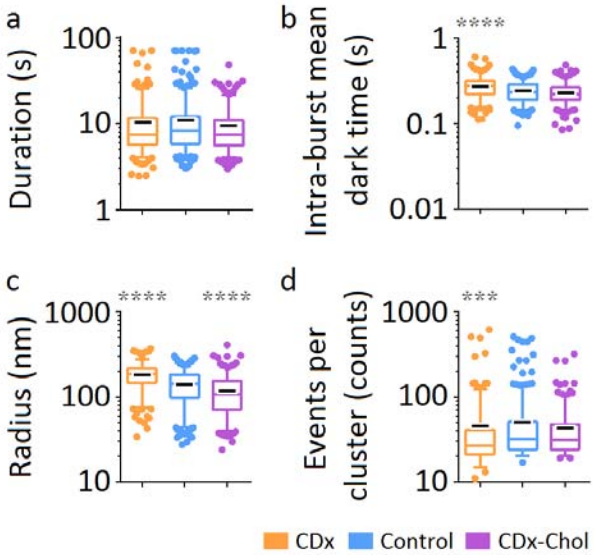

Figure 3. Real time follow up of nAChR dynamic clustering and disassembly under cholesterol depletion and enrichment. Using the live cell single-molecule localizations validated with ThunderSTORM as the input data, the qSR software (Andrews et al. 2018) was applied to obtain the nAChR clustering metrics (log scale): duration (a), intra-burst mean dark time, i.e. periods without localizations within a clustering event (b), radius (c), and number of occurrences per clustering event (d) under control and cholesterol-modifying conditions. Whiskers in box plots correspond to 95% confidence intervals; the limits indicate 75% confidence intervals; the black negative symbols indicate the mean and the colored horizontal lines the median in each case. The dots outside the intervals are outliers. Statistics: (***) and (****).

Discussion

Antibody-mediated crosslinking dramatically increases receptor immobilization

Labeling with the divalent antibody mAb35 crosslinks nAChRs, resulting in a very high proportion of immobile molecules ($\sim 80\%$) (Suppl. Fig. 2). In contrast, using the fluorescent monovalent ligand Alexa Fluor^{532} α-bungarotoxin (BTX), immobile receptors represented ~50% of the total population (Mosqueira et al. 2018). The translational motion of the remaining mAb-tagged nAChR ensemble population is heterogeneous and mostly subdiffusive. Remarkably, the generalized diffusion coefficient of the ensemble is higher in mAb-labeled nAChRs than in BTX-labeled nAChRs in both control and cholesterol-depleted conditions ($p < 0.05$) (this work and ref. (Mosqueira et al. 2018).

Apparent weak ergodicity-breaking (WEB) of nAChR diffusion

Diffusion of mAb-labeled nAChRs exhibits an ergodic-like behavior. In contrast, the diffusive behavior of BTX-labeled nAChRs is suggestive of WEB under cholesterol depletion conditions (Mosqueira et al. 2018), which we interpreted as an apparent WEB resulting from confinement or immobilization mechanisms acting on spatial- or time scales higher than that sampled for the probe within the mean recording time (i.e. mean trajectory length). A recently proposed diffusion model explains this behavior by invoking a two-state switching mechanism: when the residence times of at least one state is longer or in the order of the mean trajectory length, a single trajectory will explore only one state with a high probability, and thus it will not be representative of the ensemble, displaying an apparent WEB (Grebenkov 2019). As we have shown, nAChR diffusion is governed by alternation between two diffusional states: confined

and free. The confinement zones behave like fences with a low probability of permeation and residence times in the order of the trajectory length (hundreds of milliseconds; see Figure 1e), not allowing the particle to explore all the phase space and thus leading, in some cases, to an *apparent* weak ergodicity breaking.

mAb35-crosslinked nAChRs have longer confinement sojourns than BTX monovalently-tagged receptors

Turning angle analysis revealed anticorrelated steps, indicating that nAChRs are more likely to retrace their steps than to move forward (Figure 1 and Suppl. Fig. 5). Time lag dependence was also observed, in good agreement with numerical simulations of particles diffusing in a permeable fence model (Sadegh et al. 2017). Moreover, dissecting all trajectories into confined and free (unconfined) portions allowed us to disclose some important features of the nAChR translational behavior: it is the confined portion of the trajectories that exhibits turning angle distributions with anticorrelated steps, whereas the nearly flat distributions of the free portion of the walks correspond to Brownian diffusion (Figure 2). Thus, moving mAb-labeled nAChRs display free Brownian displacement across the cell membrane, intermittently interrupted by confinement sojourns with a well-defined length-scale, within regions of high obstacle density, that is conforming to a two-state switching diffusion model (Grebenkov 2019) with residence times comparable to the length of the trajectories. Antibody-tagged receptors exhibits longer (340-440 ms) confinement sojourns than those labeled with a monovalent ligand like α-BTX (135-257 ms) (Mosqueira et al. 2018), indicating that mAb-crosslinked receptors remain for longer periods in confined areas.

Membrane cholesterol content modulates the dynamic clustering events

In addition to the transient stopovers of individual trajectories, nAChRs also undergo dynamic cluster assembly and disassembly in a cholesterol-sensitive manner, in areas roughly 4-7-fold larger (Figure 3c). Cholesterol depletion increases their size (from radii of ∼140 nm under control conditions to ∼180 nm), whereas cholesterol enrichment reduces radii to ∼120 nm (Figure 3). When the mAb-labeled nAChR clustering events are compared with those of BTX-labeled receptors (Mosqueira et al. 2018) the former are found to have 3-fold longer lifetimes ($p < 0.01$ for control and $p < 10^{-4}$ for cholesterol-modifying conditions), a finding consistent with the idea that mAb35-induced crosslinking adds stability to the clustering events.

Implications of mAb35-nAChR complex diffusion in the framework of myasthenia

Downstream from their crosslinking step, mAbs against the MIR of the nAChR share the capacity to activate the primary physiopathological cascade induced by myasthenic autoantibodies, the so-called antigenic modulation (Conti-Tronconi et al. 1981). This process is essentially a complement-mediated focal lysis of the postsynaptic membrane (Drachman et al. 1978; Engel and Arahata 1987) that together with enhanced endocytic internalization significantly reduces cell-surface nAChR numbers. We have not only shown that the endocytic process is effectively triggered by divalent mAb35 molecules in CHO-K1/A5 cells (Kumari et al. 2008) but also that it is significantly accelerated upon cholesterol depletion (Borroni and Barrantes 2011). As shown in the present work, mAb35-mediated crosslinking results in a very high proportion of immobile receptors, while the remaining mobile ones undergo anomalous

ergodic diffusion governed by stopovers within zones of high obstacle density. Cholesterol modulates receptor diffusion, and its depletion from the membrane increases the size of the dynamic receptor clustering events. The latter may further increase nAChR degradation.

About 80% of patients with generalized myasthenia gravis have serum antibodies to the nAChR (Vincent 2002). Patients with neither anti-nAChR nor anti-MusK autoantibodies are called seronegative, and one of the hypotheses on the apparent seronegativity is that the autoantibodies of these patients react only with the membrane-associated and clustered form of the nAChR (Leite et al. 2008) as found in the native neuromuscular junction at very high densities. Here, we show that antibody-mediated nano-clustering already suffices to affect nAChR mobility.

What is the relationship between the observed cholesterol modulation of nAChR diffusion and myasthenia? Although the evidence is scanty, it has been reported that 3-hydroxy-3-methyl glutaryl coenzyme A reductase inhibitors, commonly known as statins and used therapeutically by inhibiting cholesterol biosynthesis, may trigger anti-nAChR autoantibody production (Purvin et al. 2006), and exacerbate or unmask subclinical myasthenia gravis, most often reversibly (Cartwright et al. 2004; Purvin et al. 2006) (Oh et al. 2008). We also know that cholesterol depletion reduces the number of nAChRs by accelerating the rate of endocytosis and shifting the internalization to a different endocytic pathway involving the small GTPase Arf6 (Borroni and Barrantes 2011). Moreover, we observe in this work that cholesterol depletion increases the size of nAChR clustering events. Thus, these two processes, antibody-induced clustering and cholesterol depletion-enhanced endocytosis, appear to act synergistically to ultimately decrease the cell-surface nAChR population.

Summarizing, at the single-molecule level the nAChR undergoes complex motional regimes caused by a two-state switching between free (Brownian) walks and confined diffusion within zones of high obstacle density acting as permeable fences (~34 nm radius). At the ensemble level nAChRs undergo dynamic clustering, trapping and immobilization in larger areas (~150 nm radius), which strongly depend on membrane cholesterol levels, suggesting that cholesterol-rich platforms are involved. Moreover, antibody crosslinking stabilizes both the confinement zones and clustering events. This is a clear example of how unraveling the biophysical properties of a key neurotransmitter receptor can throw light on the physiopathological basis of a disease condition, in this case the antigenic modulation characteristically observed in the autoimmune disease myasthenia gravis.

Acknowledgments

We thank Dr. Diego Krapf (Univ. of Colorado) for critical reading of the ms. Experimental work was supported by grant PIP 5205/15 from the National Scientific and Technical Research Council of Argentina (CONICET) to F.J.B.

References

Andrews, J. O., W. Conway, W. K. Cho, A. Narayanan, J. H. Spille, N. Jayanth, T. Inoue, S. Mullen, J. Thaler, and I. I. Cissé. 2018. qSR: a quantitative super-resolution analysis tool reveals the cell-cycle dependent organization of RNA Polymerase I in live human cells. *Sci Rep* 8 (1):7424.

Barrantes, F. J. 1982. Oligomeric forms of the membrane-bound acetylcholine receptor disclosed upon extraction of the Mr 43,000 nonreceptor peptide. *J.Cell Biol.* 92 (1):60-68.

Borroni, V., and F. J. Barrantes. 2011. Cholesterol modulates the rate and mechanism of acetylcholine receptor internalization. *J Biol Chem* 286 (19):17122-17132.

Burov, S., S. M. Tabei, T. Huynh, M. P. Murrell, L. H. Philipson, S. A. Rice, M. L. Gardel, N. F. Scherer, and A. R. Dinner. 2013. Distribution of directional change as a signature of complex dynamics. *Proc Natl Acad Sci U S A* 110 (49):19689-19694.

Cartwright, M. S., D. R. Jeffery, G. R. Nuss, and P. D. Donofrio. 2004. Statin-associated exacerbation of myasthenia gravis. *Neurology* 63 (11):2188.

Changeux, J. P. 2018. The nicotinic acetylcholine receptor: a typical 'allosteric machine'. *Philos Trans R Soc Lond B Biol Sci* 373 (1749).

Cisse, Ii, I. Izeddin, S. Z. Causse, L. Boudarene, A. Senecal, L. Muresan, C. Dugast-Darzacq, B. Hajj, M. Dahan, and X. Darzacq. 2013. Real-time dynamics of RNA polymerase II clustering in live human cells. *Science* 341 (6146):664-667.

Conti-Tronconi, B., S. Tzartos, and J. Lindstrom. 1981. Monoclonal antibodies as probes of acetylcholine receptor structure. 2. Binding to native receptor. *Biochemistry* 20 (8):2181-2191.

Dedecker, P., S. Duwé, R. K. Neely, and J. Zhang. 2012. Localizer: fast, accurate, open-source, and modular software package for superresolution microscopy. *Journal of Biomedical Optics* 17 (12):126008-126008.

Drachman, D. B., C. W. Angus, R. N. Adams, J. D. Michelson, and G. J. Hoffman. 1978. Myasthenic Antibodies Cross-Link Acetylcholine Receptors to Accelerate Degradation. *New England Journal of Medicine* 298 (20):1116-1122.

Engel, A. G., and K. Arahata. 1987. The membrane attack complex of complement at the endplate in myasthenia gravis. *Ann N Y Acad Sci* 505:326-332.

Golan, Y., and E. Sherman. 2017. Resolving mixed mechanisms of protein subdiffusion at the T cell plasma membrane. *Nature Communications* 8:15851.

Grebenkov, D. S. 2019. Time-averaged mean square displacement for switching diffusion. *Physical Review E* 99 (3):032133.

Janczura, J., and A. Weron. 2015. Ergodicity testing for anomalous diffusion: small sample statistics. *J Chem Phys* 142 (14):144103.

Kumari, S., V. Borroni, A. Chaudhry, B. Chanda, R. Massol, S. Mayor, and F. J. Barrantes. 2008. Nicotinic acetylcholine receptor is internalized via a Rac-dependent, dynamin-independent endocytic pathway. *J Cell Biol* 181 (7):1179-1193.

Leite, M. I., S. Jacob, S. Viegas, J. Cossins, L. Clover, B. P. Morgan, D. Beeson, N. Willcox, and A. Vincent. 2008. IgG1 antibodies to acetylcholine receptors in 'seronegative' myasthenia gravis. *Brain* 131 (Pt 7):1940-1952.

Luo, J., P. Taylor, M. Losen, M. H. de Baets, G. D. Shelton, and J. Lindstrom. 2009. Main immunogenic region structure promotes binding of conformation-dependent myasthenia gravis autoantibodies, nicotinic acetylcholine receptor conformation maturation, and agonist sensitivity. *J Neurosci* 29 (44):13898-13908.

Manzo, C., J. A. Torreno-Pina, P. Massignan, G. J. J. Lepeyre, M. Lewenstein, and M. F. Garcia-Parajo. 2015. Weak ergodicity breaking of receptor motion in living cells stemming from random diffusivity. *Physical Review X* 5:011021.

Mosqueira, A., P. A. Camino, and F. J. Barrantes. 2018. Cholesterol modulates acetylcholine receptor diffusion by tuning confinement sojourns and nanocluster stability. *Sci Rep* 8 (1):11974.

Noridomi, K., G. Watanabe, M. N. Hansen, G. W. Han, and L. Chen. 2017. Structural insights into the molecular mechanisms of myasthenia gravis and their therapeutic implications. *eLife* 6:e23043.

Oh, S. J., R. Dhall, A. Young, M. B. Morgan, L. Lu, and G. C. Claussen. 2008. Statins may aggravate myasthenia gravis. *Muscle & nerve* 38 (3):1101-1107.

Ovesný, M., P. Krizek, J. Borkovec, Z. Svindrych, and G. M. Hagen. 2014. ThunderSTORM: a comprehensive ImageJ plug-in for PALM and STORM data analysis and super-resolution imaging. *Bioinformatics* 30 (16):2389-2390.

Paz, M. L., and F. J. Barrantes. 2019. Autoimmune Attack of the Neuromuscular Junction in Myasthenia Gravis: Nicotinic Acetylcholine Receptors and Other Targets. *ACS Chemical Neuroscience* 10 (5):2186-2194.

Pissinis, D. E., C. Diaz, E. Maza, I. C. Bonini, F. J. Barrantes, R. C. Salvarezza, and P. L. Schilardi. 2015. Functional nicotinic acetylcholine receptor reconstitution in Au(111)-supported thiolipid monolayers. *Nanoscale*.

Purvin, V., A. Kawasaki, K. H. Smith, and A. Kesler. 2006. Statin-associated myasthenia gravis: report of 4 cases and review of the literature. *Medicine (Baltimore)* 85 (2):82-85.

Sadegh, S., J. L. Higgins, P. C. Mannion, M. M. Tamkun, and D. Krapf. 2017. Plasma Membrane is Compartmentalized by a Self-Similar Cortical Actin Meshwork. *Physical Review X* 7:011031.

Sikora, G., A. Wylomanska, J. Gajda, L. Sole, E. J. Akin, M. M. Tamkun, and D. Krapf. 2017. Elucidating distinct ion channel populations on the surface of hippocampal neurons via single-particle tracking recurrence analysis. *Phys Rev E* 96 (6-1):062404.

Tzartos, S., L. Langeberg, S. Hochschwender, L. W. Swanson, and J. Lindstrom. 1986. Characteristics of monoclonal antibodies to denatured Torpedo and to native calf acetylcholine receptors: species, subunit and region specificity. *J Neuroimmunol* 10 (3):235-253.

Tzartos, S. J., M. T. Cung, P. Demange, H. Loutrari, A. Mamalaki, M. Marraud, I. Papadouli, C. Sakarellos, and V. Tsikaris. 1991. The main immunogenic region (MIR) of the nicotinic acetylcholine receptor and the anti-MIR antibodies. *Mol.Neurobiol.* 5:1-29.

Tzartos, S. J., A. Kokla, S. L. Walgrave, and B. M. Conti-Tronconi. 1988. Localization of the main immunogenic region of human muscle acetylcholine receptor to residues 67-76 of the α subunit. *Proceedings of the National Academy of Sciences U.S.A.* 85:2899-2903.

Tzartos, S. J., and J. M. Lindstrom. 1980. Monoclonal antibodies used to probe acetylcholine receptor structure: localization of the main immunogenic region and detection of similarities between subunits. *Proc Natl Acad Sci U S A* 77 (2):755-759.

Tzartos, S. J., M. E. Seybold, and J. M. Lindstrom. 1982. Specificities of antibodies to acetylcholine receptors in sera from myasthenia gravis patients measured by monoclonal antibodies. *Proceedings of the National Academy of Sciences* 79 (1):188-192.

Tzartos, S. J., and A. Starzinski-Powitz. 1986. Decrease in acetylcholine-receptor content of human myotube cultures mediated by monoclonal antibodies to alpha, beta and gamma subunits. *FEBS Lett* 196 (1):91-95.

Vincent, A. 2002. Unravelling the pathogenesis of myasthenia gravis. *Nat Rev Immunol* 2 (10):797-804.

Weigel, A. V., B. Simon, M. M. Tamkun, and D. Krapf. 2011. Ergodic and nonergodic processes coexist in the plasma membrane as observed by single-molecule tracking. *Proc Natl Acad Sci U S A* 108 (16):6438-6443.

Weron, A., K. Burnecki, E. J. Akin, L. Solé, M. Balcerek, M. M. Tamkun, and D. Krapf. 2017. Ergodicity breaking on the neuronal surface emerges from random switching between diffusive states. *Sci Rep* 7 (1):5404.